J|A|C|S COMMUNICATIONS

Published on Web 10/26/2010

$CrSi_2$ Hexagonal Nanowebs

Huatao Wang,[†] Jian-Chun Wu,[‡] Yiqiang Shen,[§] Gongping Li,[†] Zhou Zhang,[†] Guozhong Xing,[†] Donglai Guo,[†] Dandan Wang,[†] Zhili Dong,[§] and Tom Wu*,[†]

Division of Physics and Applied Physics, School of Physical and Mathematical Sciences, Nanyang Technological University, Singapore 637371, Division of Chemical and Biomolecular Engineering, School of Chemical and Biomedical Engineering, Nanyang Technological University, Singapore 637459, and School of Materials Science and Engineering, Nanyang Technological University, Singapore 639798

Received July 19, 2010; E-mail: Tomwu@ntu.edu.sg

Abstract: Single-crystalline $CrSi_2$ nanostructures with a unique hexagonal nanoweb morphology have been successfully synthesized for the first time. These nanowebs span 150−200 nm and are composed of <11$\bar{2}$0> nanowire segments with a thickness of 10−30 nm. It is proposed that surface charges on the {10$\bar{1}$0} sidewalls and the minimization of electrostatic energy induce the nanoweb formation. Calculations of the electrostatic energies were used to predict the transitions between different modes of bending, which agreed well with the experimental observations.

Synthesis with control of composition, crystalline structure, and morphology is a ubiquitous goal in nanoscience and nanotechnology, enabling potential applications.[1] Advances in nanowire synthesis, ab initio materials design, and self-assembly of hierarchical nanostructures are of vital importance.[2] Recently, transition-metal silicides have attracted growing attention in fields such as electronics, photoelectrochemistry, and energy conversion.[3] Among these functional silicides, $CrSi_2$ is a notable narrow-gap semiconductor that is promising for solar cell and thermoelectric (TE) applications;[4] it is also regarded as a structural material for the aerospace industry because of its high melting point and oxidation resistance.[5] To date, there have been a few studies on $CrSi_2$ nanowires.[6] Here we report the first synthesis of single-crystalline $CrSi_2$ nanowebs, which present a fascinating nanoarchitecture and a unique formation mechanism.

We grew the $CrSi_2$ nanostructures on silicon substrates in a horizontal tube furnace via the vapor transport method [see the experimental details in the Supporting Information (SI)]. Modulation of the flow of carrier gas has been shown to effectively induce morphological and compositional changes in the general vapor-based synthesis.[7] It can change the local dynamics environment in the vicinity of the growth front, affecting the supersaturation and the simultaneous growth. In our experiments, we found that real-time adjustment of the gas flow and vapor concentration exerts a profound influence on the growth morphology of the $CrSi_2$ nanostructures (for further discussion of the role of modulated Ar flow, see the SI). As shown in the scanning electron microscopy (SEM) image in Figure 1a, $CrSi_2$ nanostructures with an unprecedented hexagonal spider-web-like morphology were observed when we abruptly ramped up the flow rate of Ar gas during growth. Their phase was confirmed by X-ray diffraction (Figure S6 in the SI). These $CrSi_2$ nanowebs usually span 150−200 nm and are composed of nanowire segments with a thickness of 10−30 nm (Figure 1b). Both clockwise and counterclockwise rotations were observed. The perspective views in Figure 1b,c suggest that these nanowebs are supported by individual perpendicular "stems" underneath, and the growth of these straight nanorod stems presumably precedes the nanoweb formation. The close-up SEM image in Figure 1d suggests that the nanowire segments in nanowebs have a rectangular cross section.

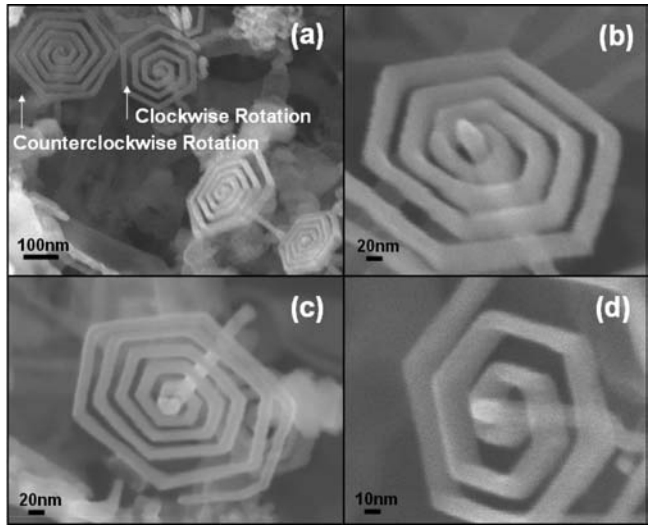

Figure 1. (a) SEM image of $CrSi_2$ nanowebs showing either clockwise or counterclockwise rotations. (b) Top view of the coherent structure. (c) Tilted view highlighting the nanorod "stem" under the nanoweb. (d) Close-up view showing the rectangular cross section.

Transmission electron microscopy (TEM) observations revealed that the nanowebs possess hexagonal symmetry (Figure 2a) and grow along the <11$\bar{2}$0> directions (Figure 2b). The sidewalls of the nanowire segments are {10$\bar{1}$0} planes. These nanowebs show high crystallinity, and no structural defects were found in the high-resolution TEM (HRTEM) images (Figure 2c,d). This structural integrity was maintained even at the turning corners (Figure S4). The calculated lattice constant (0.22 nm) and the corresponding fast Fourier transform (FFT) pattern agree well with the *C*40 structure of $CrSi_2$ (JCPDS card no. 35-0781), which was further confirmed by the energy-dispersive X-ray spectroscopy (EDS) data shown in Figure 2e−g.

The nanoweb morphology reflects the symmetry of the crystal structure of $CrSi_2$, which has a polar space group of $P6_222$ (No. 180) without a center of symmetry and is known to cause the anisotropic TE properties in bulk single crystals.[8] An important attribute of this particular crystal structure is that it presumably

[†] School of Physical and Mathematical Sciences.
[‡] School of Chemical and Biomedical Engineering.
[§] School of Materials Science and Engineering.

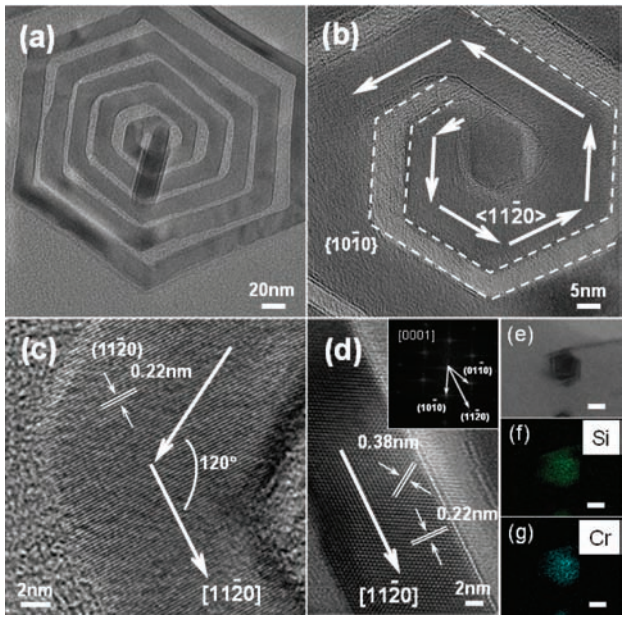

Figure 2. (a, b) Typical TEM images of $CrSi_2$ nanowebs with the growth directions along <11$\bar{2}$0> and sidewalls of {10$\bar{1}$0} planes. (c, d) HRTEM images taken along the *c* zone axis on the turning corner and the nanowire segment. The inset in (d) is the corresponding FFT pattern. (e−g) EDS element maps of a $CrSi_2$ nanoweb. The scale bars represent 100 nm.

gives charged {10$\bar{1}$0} crystalline planes (Figure 3a and Figure S8; also see the additional discussion in the SI),[9] that is, the corresponding sidewalls in each nanowire segment are oppositely charged (see the Figure 3e inset). The associated electrostatic interaction and the energy minimization are closely linked with the nanoweb formation, as in the formation mechanism proposed for ZnO nanohelixes, nanosprings, and nanorings.[10] Zhou et al.[11] also found that the crystal structure and surface atomic arrangement play key roles in forming silicide nanostructures. Figure 3b simulates the intensity contours of the electric field induced by the charged sidewall planes near an isolated nanoweb corner, and the electrostatic interactions generated by these charged sidewalls presumably modulate the growth directions during formation of the nanoweb. Figure 3e depicts the possible situations of bending with different angles between the adjacent segments. These four possibilities preserve the preferred {10$\bar{1}$0} crystalline surfaces. In addition to the most frequent 120° bending between segments (bending I in Figure 3e), which gives the regular hexagonal nanowebs, we also observed 60° bending (bending II), which switches the nanoweb rotation from counterclockwise to clockwise (Figure 3c) or vice versa (Figure 3d). For the other possible types of bending shown in Figure 3e, bending IV, which could give zigzag nanowires, was seldom observed,[12] and bending III corresponding to straight growth was also rare.

These observations are consistent with the scenario that the electrostatic interaction dictates the growth. Figure 3f shows a comparison of the electrostatic energies ($E_{electro}$) for bendings I, II, and III (for calculation details, see the SI), which reveals the critical role of the distance *d* between the parallel segments. If *d* is less than a critical value, which was estimated to be 16−25 nm in our case, bending I has the minimum electrostatic energy; otherwise the energy of bending II is the lowest. Bending III always has the highest energy. The experimental results are consistent with the model, as shown in a couple of examples here: in Figure 3c, the nanoweb switches from bending I to bending II when *d* changes from 17 nm (d_1) to 29 nm (d_2), and Figure 3d shows another case where *d* increases from 11 nm (d_3) to 17 nm (d_4) and then to 19 nm (d_5), preceding the expected transition. Furthermore, when such transitions between different bending angles occurred near the nanoweb center during the early growth stage, forklike morphologies were often observed (for more details, see the SI).

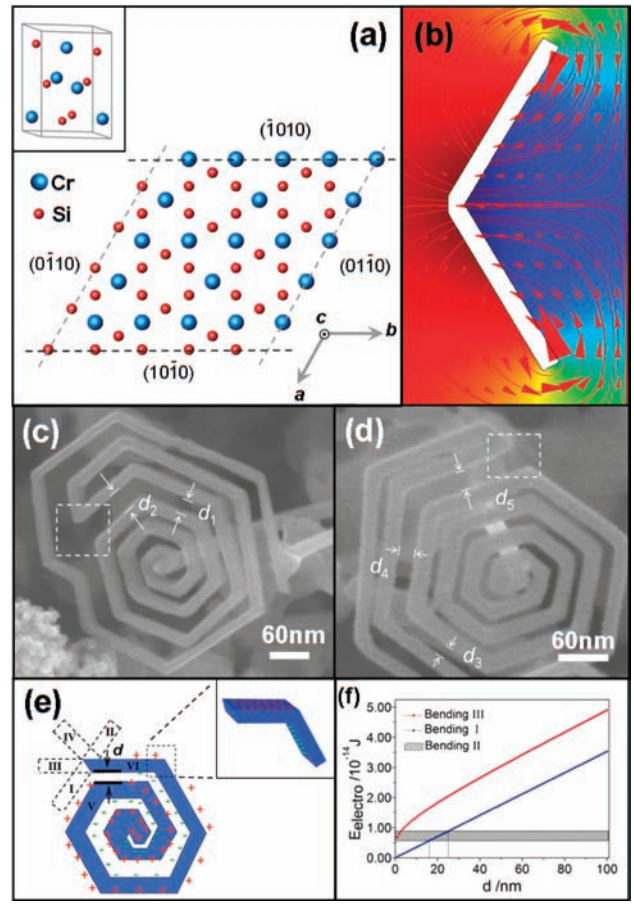

Figure 3. (a) Plane view of the crystal structure of *C*40 $CrSi_2$ along the *c* axis, showing the positively or negatively charged {10$\bar{1}$0} planes. The inset shows the unit cell. (b) Simulated electric field intensity contours around one nanoweb corner. (c, d) SEM images of nanowebs showing transitions between bendings I and II. (e) Schematic of a nanoweb illustrating all possible types of bending at its end that preserve the equivalent sidewalls. The inset depicts the charged sidewalls at a nanoweb corner. (f) Influence of the distance between parallel segments on the electrostatic energies of various types of bending.

In conclusion, single-crystalline $CrSi_2$ nanowebs with high structural integrity and unique morphology have been synthesized for the first time. The growth is likely driven by the minimization of electrostatic energy associated with the charged sidewalls. This new member of the family of silicide nanostructures may find analogies in other materials systems and facilitate the construction of functional nanodevices.

Acknowledgment. T.W. thanks NTU (SUG 20/06) and MOE (RG 46/07) for support.

Supporting Information Available: Experimental details of the synthesis of $CrSi_2$ nanowebs, straight nanowires, and zigzag nanowires; SEM images; XRD pattern of as-synthesized nanowebs; TEM images of nanoweb centers; HRTEM image of a nanoweb corner; discussion of forklike nanowebs; atomic model of $CrSi_2$ depicted along the *a* axis; and the calculation of the electrostatic energy. This material is available free of charge via the Internet at http://pubs.acs.org.

References

(1) (a) Lauhon, L. J.; Gudiksen, M. S.; Wang, C. L.; Lieber, C. M. *Nature* **2002**, *420*, 57–61. (b) Caroff, P.; Dick, K. A.; Johansson, J.; Messing, M. E.; Deppert, K.; Samuelson, L. *Nat. Nanotechnol.* **2009**, *4*, 50–55. (c) Gudiksen, M. S.; Lauhon, L. J.; Wang, J.; Smith, D. C.; Lieber, C. M. *Nature* **2002**, *415*, 617–620. (d) Kuykendall, T.; Pauzauskie, P. J.; Zhang, Y.; Goldberger, J.; Sirbuly, D.; Denlinger, J.; Yang, P. *Nat. Mater.* **2004**, *3*, 524–528.

(2) (a) Xia, Y.; Yang, P.; Sun, Y.; Wu, Y.; Mayers, B.; Gates, B.; Yin, Y.; Kim, F.; Yan, H. *Adv. Mater.* **2003**, *15*, 353–389. (b) Tian, B.; Xie, P.; Kempa, T. J.; Bell, D. C.; Lieber, C. M. *Nat. Nanotechnol.* **2009**, *4*, 824–829.

(3) (a) Schmitt, A. L.; Higgins, J. M.; Szczech, J. R.; Jin, S. *J. Mater. Chem.* **2010**, *20*, 223–235. (b) Chen, L. J. *JOM* **2005**, *57*, 24–30. (c) Chang, M. T.; Chen, C. Y.; Chou, L. J.; Chen, L. J. *ACS Nano* **2009**, *3*, 3776–3780. (d) Higgins, J. M.; Schmitt, A. L.; Guzei, I. A.; Jin, S. *J. Am. Chem. Soc.* **2008**, *130*, 16086–16094. (e) Liu, B.; Wang, Y.; Dilts, S.; Mayer, T. S.; Mohney, S. E. *Nano Lett.* **2007**, *7*, 818–824. (f) Varadwaj, K. S. K.; Seo, K.; In, J.; Mohanty, P.; Park, J.; Kim, B. *J. Am. Chem. Soc.* **2007**, *129*, 8594–8599. (g) Lin, Y.; Zhou, S.; Liu, X.; Sheehan, S.; Wang, D. *J. Am. Chem. Soc.* **2009**, *131*, 2772–2773. (h) Zhao, A.; Zhang, X.; Chen, X.; Guan, J.; Liang, C. *J. Phys. Chem. C* **2010**, *114*, 3962–3967. (i) Zhou, S.; Liu, X.; Wang, D. *Nano Lett.* **2010**, *10*, 860–863. (j) Dong, L.; Bush, J.; Chirayos, V.; Solanki, R.; Jiao, J.; Ono, Y.; Conley, J. F.; Ulrich, B. D. *Nano Lett.* **2005**, *5*, 2112–2115.

(4) (a) Mattheiss, L. F. *Phys. Rev. B* **1991**, *43*, 12549–12555. (b) Anderson, W. A.; Delahoy, A. E.; Milano, R. A. *J. Appl. Phys.* **1974**, *45*, 3913–3915. (c) Zhou, F.; Szczech, J.; Pettes, M. T.; Moore, A. L.; Jin, S.; Shi, L. *Nano Lett.* **2007**, *7*, 1649–1654.

(5) Murarka, S. P. *J. Vac. Sci. Technol.* **1980**, *17*, 775–792.

(6) (a) Seo, K.; Varadwaj, K. S. K.; Cha, D.; In, J.; Kim, J.; Park, J.; Kim, B. *J. Phys. Chem. C* **2007**, *111*, 9072–9076. (b) Szczech, J. R.; Schmitt, A. L.; Bierman, M. J.; Jin, S. *Chem. Mater.* **2007**, *19*, 3238–3243. (c) Yu, L.; Ma, Y.; Zhu, J.; Feng, H.; Wu, Q.; Lu, Y.; Lin, W.; Sang, H.; Hu, Z. *J. Phys. Chem. C* **2008**, *112*, 5865–5868.

(7) Lilach, Y.; Zhang, J. P.; Moskovits, M.; Kolmakov, A. *Nano Lett.* **2005**, *5*, 2019–2022.

(8) (a) Hahn, T. *International Tables for Crystallography*; Springer: New York, 2006; Vol. A, pp 804−808. (b) Nishida, I. *J. Mater. Sci.* **1972**, *7*, 1119–1124.

(9) (a) Dasgupta, T.; Etourneau, J.; Chevalier, B.; Matar, S. F.; Umarji, A. M. *J. Appl. Phys.* **2008**, *103*, 113516. (b) Gottlieb, U.; Laborde, O.; Thomas, O.; Rouault, A.; Senateur, J. P.; Madar, R. *Appl. Surf. Sci.* **1991**, *53*, 247–253. (c) Noguera, C. *J. Phys.: Condens. Matter* **2000**, *12*, R367–R410.

(10) (a) Kong, X. Y.; Wang, Z. L. *Appl. Phys. Lett.* **2004**, *84*, 975–977. (b) Kong, X. Y.; Ding, Y.; Yang, R.; Wang, Z. L. *Science* **2004**, *303*, 1348–1351. (c) Kong, X. Y.; Wang, Z. L. *Nano Lett.* **2003**, *3*, 1625–1631. (d) Gao, P. X.; Ding, Y.; Mai, W.; Hughes, W. L.; Lao, C.; Wang, Z. L. *Science* **2005**, *309*, 1700–1704.

(11) Zhou, S.; Liu, X.; Lin, Y.; Wang, D. *Chem. Mater.* **2009**, *21*, 1023–1027.

(12) (a) Duan, J.; Yang, S.; Liu, H.; Gong, J.; Huang, H.; Zhao, X.; Zhang, R.; Du, Y. *J. Am. Chem. Soc.* **2005**, *127*, 6180–6181. (b) Wang, H.; Liu, G.; Yang, W.; Lin, L.; Xie, Z.; Fang, J. Y.; An, L. *J. Phys. Chem. C* **2007**, *111*, 17169–17172.

JA106402P